Shock Waves (2024) 34:181–192
https://doi.org/10.1007/s00193-024-01185-2

ORIGINAL ARTICLE

Air-breathing rotating detonation engine supplied with liquid kerosene: propulsive performance and combustion stability

W. Perkowski[1] · A. Bilar[1] · M. Augustyn[1] · M. Kawalec[1]

Received: 17 October 2023 / Revised: 14 May 2024 / Accepted: 16 May 2024 / Published online: 2 July 2024

Abstract
Experimental results are presented for a rotating detonation engine supplied with liquid kerosene and preheated air without liquid or gaseous additions to the propellant mixture. Various combustion modes for the generic combustor geometry design were observed—from deflagration, through pulsed combustion and high-frequency instabilities, to stable detonation propagation. Attention was paid to detonation stability (if present), its characteristics, and the propulsive performance of the combustor with a focus on specific thrust and pressure gain through thrust and outlet total pressure measurement. These parameters measured for the observed modes were compared. The stability of the detonation combustion proved not to be critical to achieve high performance of the combustion chamber. For example, high performance was achieved for combustion modes with high-frequency instabilities.

Keywords Detonation · RDE · Liquid fuels · Kerosene detonation · Air-breathing RDE

1 Introduction

The application of the rotating detonation waves for propulsion opens up new design possibilities. It allows to design smaller, lighter, and shorter combustion chambers [1]. However, major flow problems are apparent at this research stage. The majority of research in this field focuses on the concept of rotating detonation engines (RDEs), where the advantage is the higher thermodynamic efficiency of combustion at increased pressure. Moreover, the increased pressure in the combustion chamber increases the total pressure of the flow as a result of detonative combustion [2]. Kaemming and Paxson [3] described a quantitative method of determining pressure gain by calculating the equivalent available pressure (EAP) value, which is currently a widely used method in comparing capabilities of achieving pressure gain for detonative engine setups, while Bach et al. [4] compared it with empirical methods. A vast number of chamber geometries, injector designs, and propellant mixtures have been investigated; however, there is still a lack of experimental evidence for achieving pressure gain. Moreover, relative flow losses are usually significant [5, 6]. Another problem is that up to now mostly gaseous fuels (with a major focus on hydrogen) have been used as the propellant. A number of studies have investigated stability of the detonation wave both experimentally and numerically in the development of RDEs as a valid propulsion system [6–11]. Since gaseous fuels may not be suitable for the aerospace industry, an air-breathing RDE with the detonation combustion of liquid fuels must be achieved. So far, several studies have been published using kerosene as a fuel for detonation air-breathing engines [12]. Most often, however, the use of kerosene required additional injection of oxygen or hydrogen to achieve detonation operation [8, 12–15]. In this paper, we aimed to present experimental work done on a detonative combustion chamber supplied only with liquid kerosene and hot air. Extensive research has been made with generic geometrical configurations allowing

Communicated by G. Ciccarelli.

This paper is based on work that was presented at the 29th International Colloquium on the Dynamics of Explosions and Reactive Systems (ICDERS), Siheung, Korea, July 23–28, 2023.

✉ M. Kawalec
michal.kawalec@ilot.lukasiewicz.gov.pl

W. Perkowski
witold.perkowski@ilot.lukasiewicz.gov.pl

A. Bilar
adam.bilar@ilot.lukasiewicz.gov.pl

M. Augustyn
maksymilian.augustyn@ilot.lukasiewicz.gov.pl

[1] Łukasiewicz - Institute of Aviation, Warsaw, Poland

to capture a variety of combustion modes including stable detonation, deflagration, deflagration with high-frequency instabilities (HFIs) [16], and pulsed combustion mode [17]. The work includes the analysis of the propulsive performance of the engine and a comparison between various combustion modes and factors affecting it.

2 Experimental setup

2.1 Experimental facility

2.1.1 Combustion chamber geometries

The process of fuel–air propellant mixture preparation is crucial to the development of a liquid-fueled RDE. The generic continuously rotating detonation (CRD) chamber ($D = 141$ mm outer diameter) schematic with description is presented in Fig. 1. The dimensions of inlet $A3.1 = 1500$ mm^2 and combustion chamber $A3.2 = 10{,}700$ mm^2 ($h = 31$ mm) cross sections as well as the chamber length ($L = 125$ mm) were fixed. However, it was uncertain whether propulsive performance for the cases of deflagration combustion was affected by incomplete combustion in such a short chamber; therefore, additional experiments were done for the same cross section but with an extended chamber length ($L = 276$ mm).

A key factor for achieving various combustion modes was controlling the average velocity through the combustion chamber. This velocity was adjusted by changing the $A8$ cross-sectional area (see Fig. 1). The $A8/A3.1$ ratio varied from 1.48 to 1.85.

The geometrical parameters of the cross section are marked in Fig. 1 using the same naming convention popular in the scientific community [3–6, 18]. The combustion chamber had a simple slit convergent outlet nozzle without a divergent part. In this research, fuel injector based on 48 holes with a diameter of $\phi = 0.22$ mm was located about 25 mm before the combustion chamber inlet slit at axial position 3.1.

2.1.2 Air supply system

The experimental test stand with its various components is provided in Fig. 2. The test stand was equipped with a thermally insulated 2-m^3 air tank for up to 10 bar pressure and up to 200 °C temperature. It fed the experimental combustion chamber through two valves—a manual ball valve and a fast-response controlled valve. The apparatus allowed for the supply of up to 1.5 kg/s of air at 180 °C to the combustion chamber.

The test stand with the basic components is highlighted in Fig. 3. The combustion chamber under test is presented in Fig. 4.

2.1.3 Liquid fuel supply system

Pressure-fed system was used to supply liquid fuel from the 3-dm^3 tank to the chamber, see Fig. 2. Fuel was pressurized with nitrogen or air at up to 100 bar. Aviation-grade kerosene Jet-A1 was chosen as a fuel and fed to the chamber through a mass flow meter and electromagnetic valve. During the tests, supply pressures of 30–40 bar were used. It is known that some of the nitrogen used to pressurize the fuel system dissolves in the kerosene [19]; it is estimated that the maximum nitrogen mole fraction in kerosene is less than 1%. Fuel is injected just before the combustion chamber at a 30-degree angle against the flow (see Fig. 1). The injector is equipped with 0.3-mm-diameter equally spaced injection holes. The

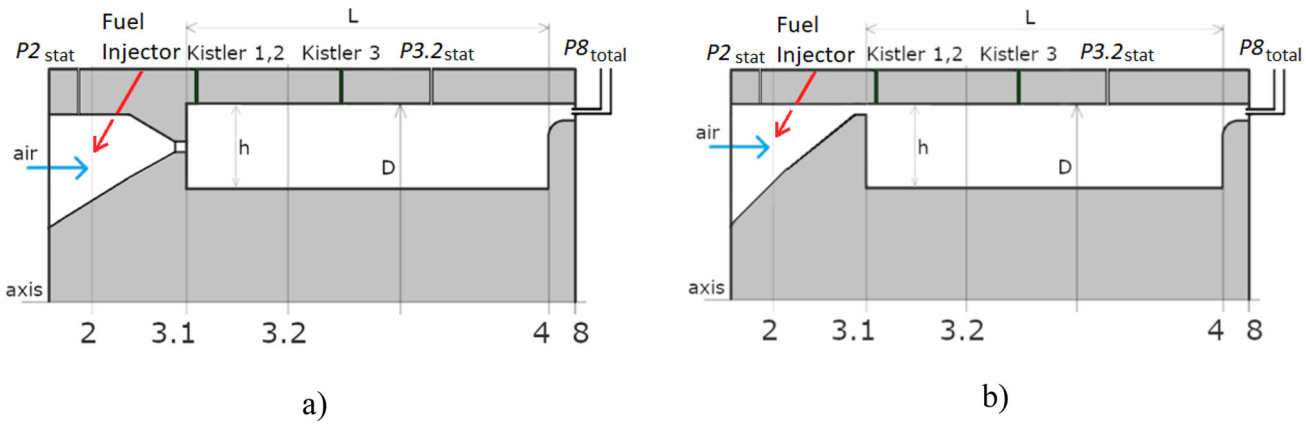

Fig. 1 Schematic showing the generic 141-mm-outer-diameter CRD chamber with fuel injector and pressure measurement positions. Two variants of the fuel–air introduction into the combustion chamber were tested: **a** fuel introduced halfway up the combustion chamber channel (variant A); **b** the introduction of the mixture just at the outer diameter of the channel (variant B). Both variants have the same 1500-mm^2 inlet slit at axial position 3.1 and combustion chamber cross section. Kistler 2 is circumferentially located in the same plane as Kistler 1

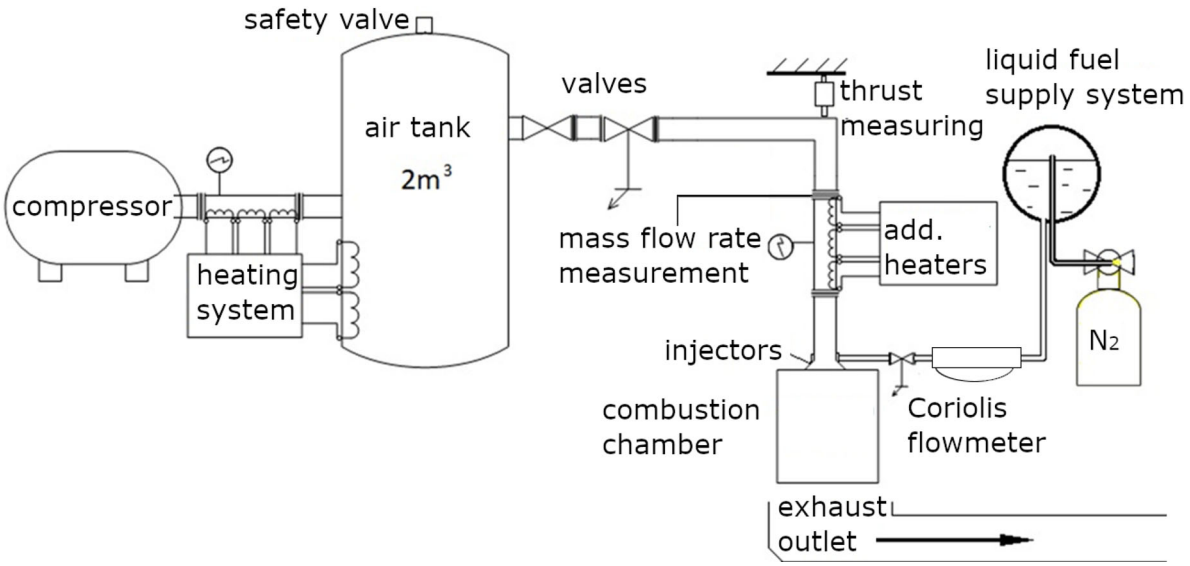

Fig. 2 Schematic showing the air and kerosene supply systems

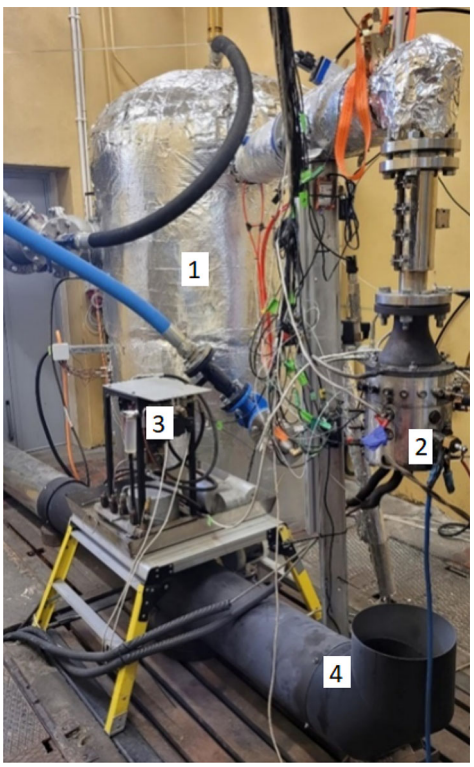

Fig. 3 Photograph of the test stand. 1—Main tank, 2—combustion chamber, 3—fuel supply system, and 4—exhaust outlet

Fig. 4 Combustion chamber and the exhaust

experience of kerosene droplet atomization tests was used [20]. The injection speed was about 30–40 m/s, approximate SMD (Sauter mean diameter) was 8.9 μm.

2.1.4 Ignition system

A pyrotechnic black powder-based initiator was used to initiate combustion. The initiator was triggered by an electrical impulse applied to a standard percussion cap.

2.1.5 Measurement and data acquisition system

The data acquisition system based on National Instruments (NI) architecture consisted of the NI USB 6366 card with 1 MHz sampling frequency. The pressure measurement range for Kistler 603CAB transducers was set to 0–25 bar with an uncertainty of $\pm 1\%$. Control of the test facility was achieved via a USB 6259 card and NI USB 6366 for recording high-frequency pressure measurements. The electric signal for ignition was delayed for 700 ms relative to the start of the fuel and air supply in order to achieve steady conditions of flow and temperature.

The air mass flow was measured by a metering orifice (calibrated for a specific range of mass flow rate), while the fuel mass flow rate was measured by a Coriolis flow meter (type FCB430 Coriolis with measuring range from 0.02 to 8000 kg/h $\pm 0.4\%$).

The thrust generated by the combustion chamber is measured indirectly by a load cell (type KM1503 with measuring range from 0 up to 4900 N $\pm 0.1\%$), which is connected with preload between the ceiling and the pipeline that features adequate stiffness for the purpose (Fig. 2).

The combustion chamber's plenum featured static pressure ($P2_{\mathrm{stat}}$) and temperature ($T2$) measurements upstream of the chamber inlet slit, see Fig. 1. Inside the combustion chamber, fast pressure changes (in the main channel close to the 3.1 section) were measured by piezoelectric sensors Kistler 603 CAB. The static pressure ($P3.2_{\mathrm{stat}}$) was also measured at several points along the chamber and outlet total pressure ($P8_{\mathrm{total}}$) probe.

2.2 Description of experiments

Experiments were set up for similar mass flow rate and similar equivalence ratio (ER) ranges. All flow conditions were adjusted to achieve the desired mass flow rate and equivalence ratio during combustion; these parameters varied considerably (up to 30%). Immediately after ignition when the system was cold, the mixture was leaner (close to stoichiometry), and during heat-up, it became richer, finally achieving the desired value. Experiments lasted 2 s, but combustion only lasted 0.8 s. The average values were sampled from time $t = 0.9$ s to $t = 1.1$ s, while valves opened at $t = 0$, ignition occurred at $t = 0.8$ s, and valve closure—at $t = 2$ s.

In experiments, the pressure gain was estimated according to the formula:

$$\mathrm{PG} = \frac{P8_{\mathrm{total}} - P2_{\mathrm{total}}}{P2_{\mathrm{total}}} \quad . \tag{1}$$

The modification of the $A8$ area affects pressure loss between $A2$ and $A3.2$. These losses are the largest component of flow losses through the combustion chamber. Enlargement of the $A8$ area results in greater flow losses.

The $P2_{\mathrm{stat}}$ was a static pressure measurement in the chamber plenum (see Fig. 1). Due to the very low axial flow velocity of 20–25 m/s, the difference between static pressure and total pressure was lower than 0.5%; therefore, it was assumed that $P2_{\mathrm{stat}} \approx P2_{\mathrm{total}}$. The pressure gain determined through EAP methodology [2] is based on the outlet total pressure estimation from the thrust measurement where base drag is also considered. According to Brophy et al. [5] and Kaemming [2], the base drag is measured to account for about 12% of total thrust for comparable geometry design and flow conditions; however, it was not measured and taken into account in this work.

The specific thrust (F_{s}) was calculated by:

$$F_{\mathrm{s}} = \frac{\mathrm{Thrust}}{\dot{m}_{\mathrm{air+fuel}}}, \tag{2}$$

where the $\dot{m}$ is the mass flow rate. This parameter was critical for the comparison of different combustion modes.

3 Results

Experiments performed on this combustion chamber highlighted various combustion modes. Fast deflagration through longitudinally pulsed detonation instabilities, high-frequency instabilities, and both stable detonation and unstable detonation were observed. Certain combustion modes were evaluated based on research reported by Anand et al. [16, 17] and Wang et al. [21]. In these papers, various combustion modes were described and their influence on propulsive performance was evaluated.

All tests were performed with as similar flow parameters as possible, e.g., an attempt was made to achieve a total mass flow rate of about 1.2 kg/s. The mixture composition at which different modes were observed varied. Deflagration was achieved for compositions close to stoichiometric, while the other modes were observed at ER = 1.3.

Pressure peak measurements from the high-frequency sensors were subjected to FFT analysis to determine detonation wave stability. Wave numbers and direction were determined from two pressure sensors positioned in one plane and aligned 120 degrees to each other. Imaging methods were not used, i.e., no high-speed camera was used in the vertical layout of the combustion chamber outlet for safety reasons, when using kerosene.

3.1 Deflagration

The high-frequency pressure measurements for the deflagration mode of operation are provided in Fig. 5. This pressure

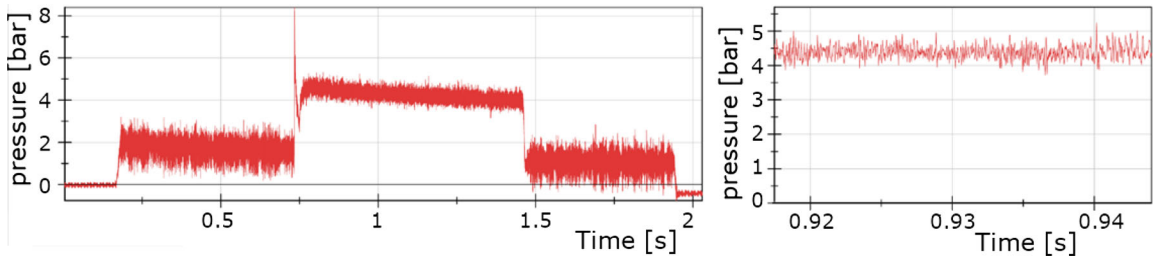

Fig. 5 Pressure recordings with high-frequency sensor and zoomed part of the trace during combustion. Average static pressure in the combustion chamber $p = 4.5$ bar; thrust $F = 1148$ N; $\dot{m}_{\text{total}} = 1.29$ kg/s; ER $= 0.91$; $A8/A3.1 = 1.81$

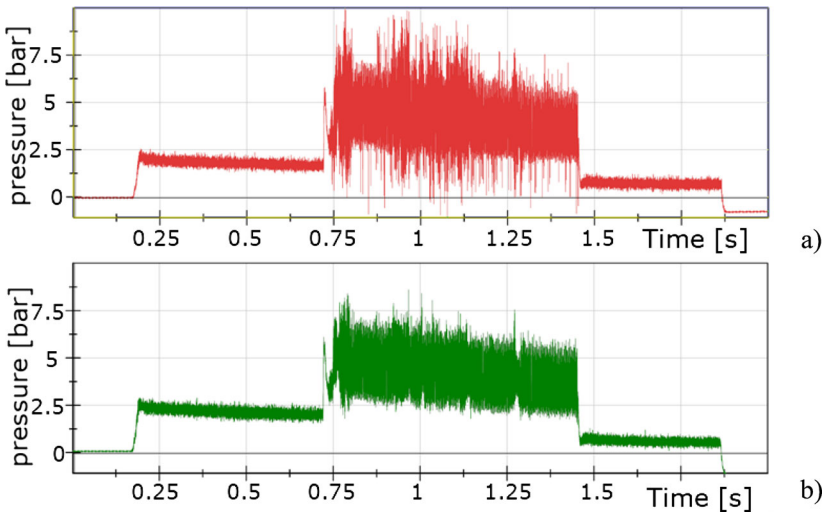

Fig. 6 Pressure measured with 1 MHz (high frequency) transducers **a** Kistler 1, **b** Kistler 2. Average static pressure in the combustion chamber $p = 5.32$ bar; thrust $F = 1256$ N; $\dot{m}_{\text{total}} = 1.19$ kg/s; ER $= 1.41$; $A8/A3.1 = 1.48$

signal is typical of the deflagration mode, it is smooth, and no pressure peaks were recorded. In this mode, the combustion chamber was presumably too short; hence, the combustion was not complete and choking of the flow was minor. The specific thrust was about 800 m/s (Fig. 20). Deflagrative combustion was achieved for combustion chamber geometry shown in Fig. 1a for outlet slit area ratio $A8/A3.1 = 1.81$. The deflagration mode was not observed in the variant of the combustion geometry shown in Fig. 1b.

As an exception, deflagration was achieved for the longer combustion chamber geometry ($L = 276$ mm) where the specific thrust was 20% greater than for the deflagration with the same flow conditions in the shorter combustion chamber. This demonstrates the inherent difficulty in comparing the deflagration to detonation modes where the former requires a much longer combustion chamber to combust the majority of the propellant. However, this point is not discussed in this paper; the analysis is focused on the geometry described in Fig. 1.

3.1.1 Low-frequency instabilities

This type of instability occurred most frequently for geometry configuration with area ratio $A8/A3.1 = 1.48$ for both variants (outer inlet slit and middle inlet slit) shown in Fig. 1. Pressure probes were placed axially and circumferentially in one plane, and their records did not show any time shift between each other; hence, there was no specific wavefront propagating in a specified direction in the chamber. For such instabilities, pressure transducers registered relatively high amplitudes of 4–6 bar and oscillations at around 450–550 Hz (Figs. 6, 7). Strong pulsations were observed of the airflow in the whole supply system.

The specific thrust did not exceed 1100 m/s and the calculated pressure gain settled from −9 to −25% (where negative PG means total pressure losses (Fig. 20).

3.1.2 High-frequency instabilities (HFIs)

Under certain circumstances, i.e., particular combination of geometry configuration and flow conditions), quasi-stable detonation combustion occurs. According to Anand et al. [16], this has been identified as high-frequency instabilities (HFIs). In such experiments in an unthrottled combustion chamber, the pressure signal oscillated with high frequencies and fairly large amplitudes around the average pressure in the combustion chamber. The shape of pulses were acoustic-like and sometimes more like detonation waves. In experiments conducted by the authors, similar pressure behavior in the combustion chamber was observed (Fig. 8). The recorded

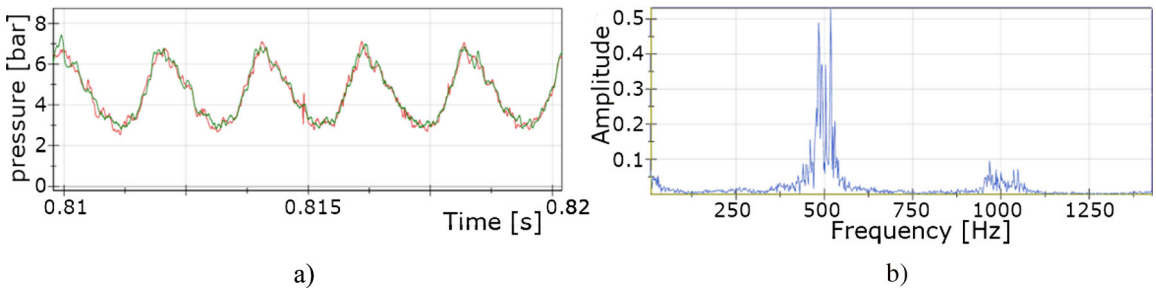

Fig. 7 Zoom-in of the pressure measurement in Fig. 6 (**a**) and corresponding wave frequency spectrum (**b**)

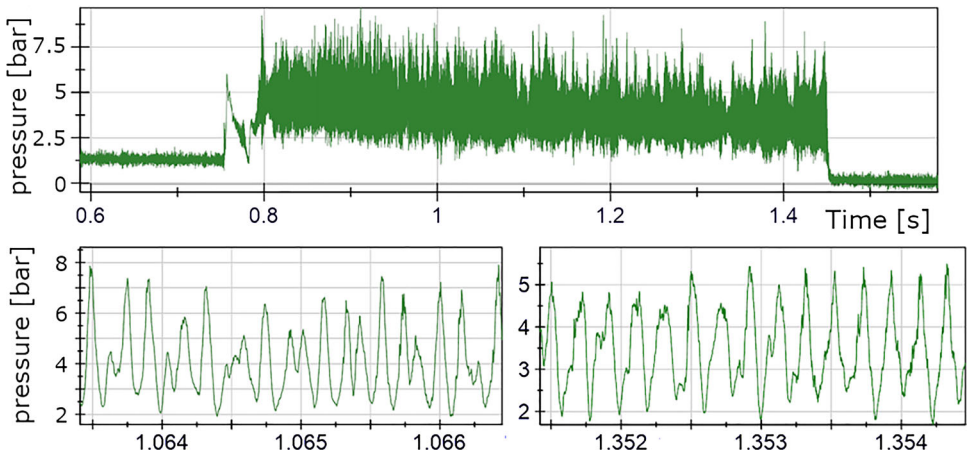

Fig. 8 Pressure measurement in the combustion chamber and two zoomed-in sectors highlighted. Average static pressure in the combustion chamber $p = 5.07$ bar; thrust $F = 1343$ N; $\dot{m}_{\text{total}} = 1.16$ kg/s; ER $= 1.3$; $A8/A3.1 = 1.66$

frequencies suggest the appearance of waves propagating at a speed of about 800–1000 m/s, which is around the speed of sound in hot combustion gases.

Several factors prevented us from identifying such pressure records as evidence of detonative combustion. Firstly, the shape of pressure peaks considerably differed from what is recognized and comparable with sharp pressure peaks associated with detonation wave passage. Secondly, the wave reached only around 50–60% of Chapman–Jouguet velocity (V_{C-J} about 1800 m/s [22, 23]). Such a combustion mode was mostly achieved for $A8/A3.1 = 1.66$.

Deflagration with HFI featured a pressure signal similar to acoustic waves with an amplitude of 4–10 bar at a dominant frequency of 5 kHz with sub-harmonic of 2.5 kHz and higher harmonics above around 7.4 kHz and more, see in Fig. 9. It is assumed that waves propagating at high speed (800–1000 m/s) occur during deflagrative combustion.

The specific thrust in HFI mode was 1200–1300 m/s, and calculated pressure gain settled from −9 to −21% (Fig. 20).

3.1.3 Stable detonation

Stable CRD was achieved only for a narrow range of equivalence ratios and by adjusting the outlet slit width, as described in Sect. 2.1.1. The process requires a considerably high velocity of fresh propellant inflow which in turn accounted for hindered combustion initiation. The recorded detonative combustion process featured high wave speed (around 70% of V_{C-J}) with characteristic sharp pressure peaks and high-pressure amplitudes (Figs. 10, 11).

The recorded detonative combustion process featured high wave speed with characteristic sharp pressure peaks and high-pressure amplitudes (see Fig. 11). The FFT in Fig. 12 shows a narrow range of dominant frequency.

In this work, stable CRD was recorded only for Variant A geometry (see Fig. 1). In the laboratory, the stable detonation was achieved also for other variants of chamber geometry, including a modified version of Variant A; however, they

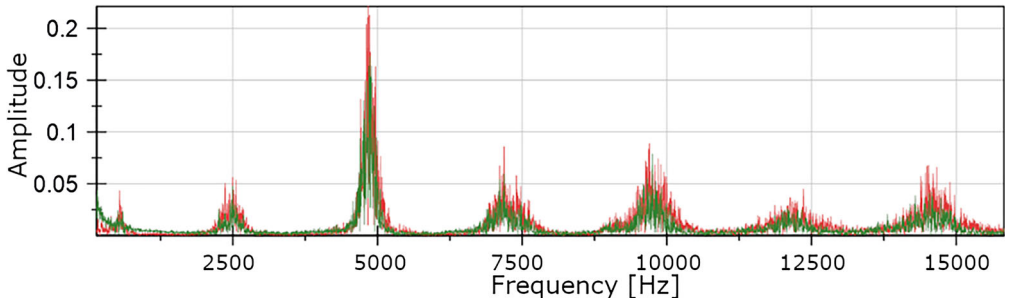

Fig. 9 Wave frequency spectrum (amplitude vs. frequency) for the pressure signal in Fig. 8

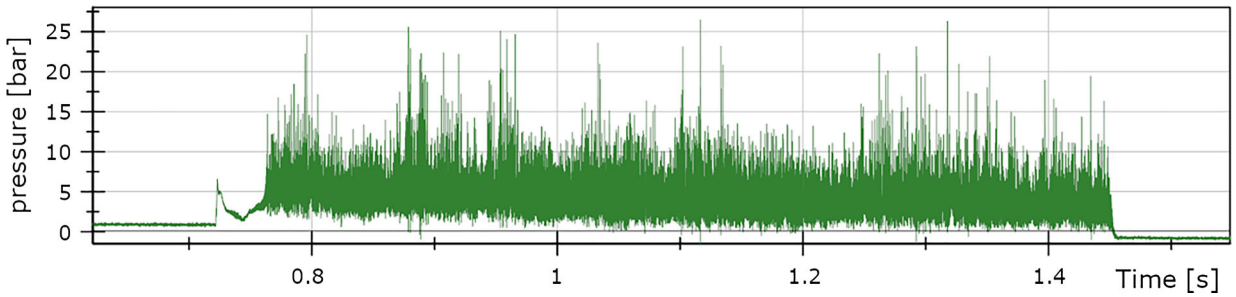

Fig. 10 Pressure measurement in the combustion chamber. Average static pressure in the combustion chamber $p = 4.7$ bar; thrust $F = 1386$ N; $\dot{m}_{\text{total}} = 1.17$ kg/s; ER $= 1.29$; *A8/A3.1* $= 1.85$

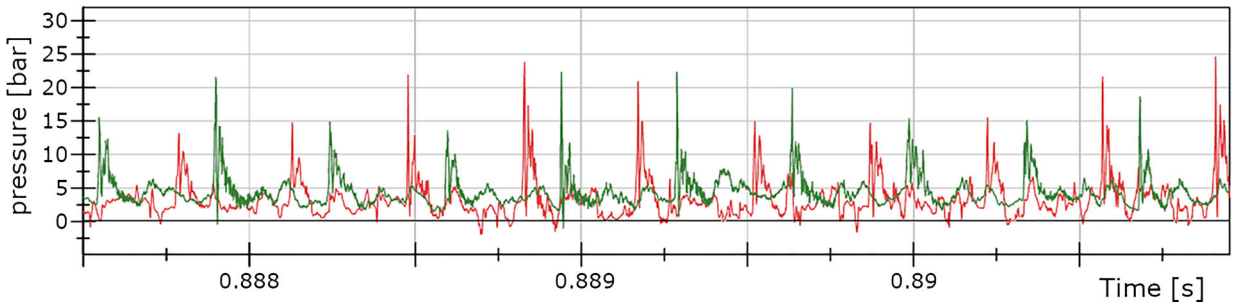

Fig. 11 Pressure measurement in the combustion chamber (zoomed record for signal in Fig. 10)—overlapping Kistler 1 and 2 records

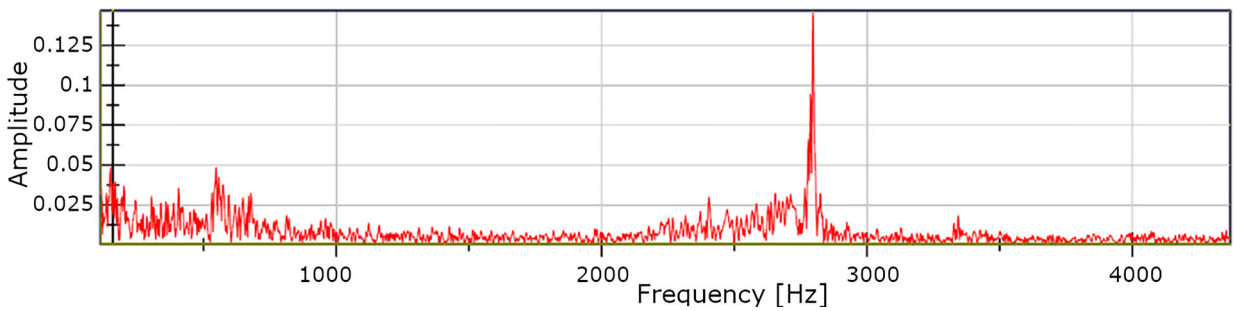

Fig. 12 Wave frequency spectrum (amplitude vs. frequency) for pressure measurement in Fig 10

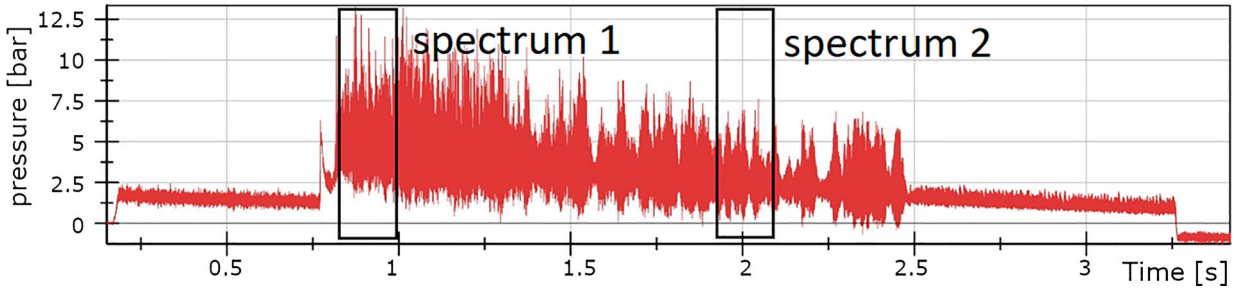

Fig. 13 Pressure measurement in the combustion chamber. Average static pressure in the combustion chamber $p = 4.7$ bar; thrust $F = 1390$ N; $\dot{m}_{\text{total}} = 1.1$ kg/s; ER $= 1.33$ (for spectrum 1) and ER $= 1.43$ (for spectrum 2); $A8/A3.1 = 1.85$

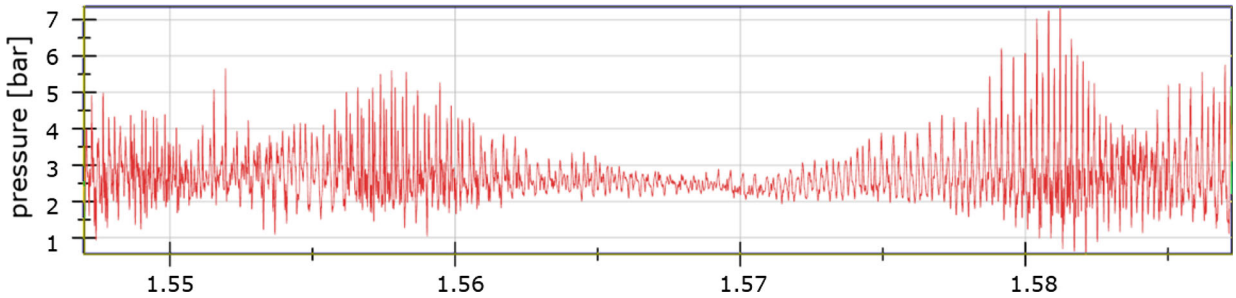

Fig. 14 Zoomed-in pressure record from Fig. 13 showing unstable detonation

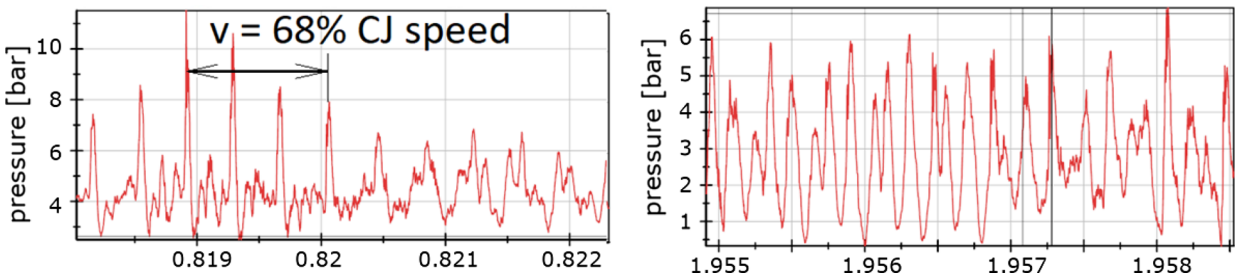

Fig. 15 Zoomed-in pressure record from Fig. 13 for the region labeled "spectrum 1" (left) and "spectrum 2" (right)

were not included in the analysis in this paper for convenience and unambiguity of comparison. For kerosene–air, it required a high velocity of fresh propellant inflow. Stable detonation was achieved mostly for $A8/A3.1$ greater than 1.85. It was achieved by increasing the outlet cross-sectional area ($A8$) which in turn increased the pressure drop between the plenum and chamber through the inlet slit (resulting in PG $= -21\%$). However, specific thrust reached the level up to 1300 m/s (see Fig. 20).

3.1.4 Transition states

The tests repeatedly showed operation in an undefined mode, where the recorded pressure records showed a change in com-

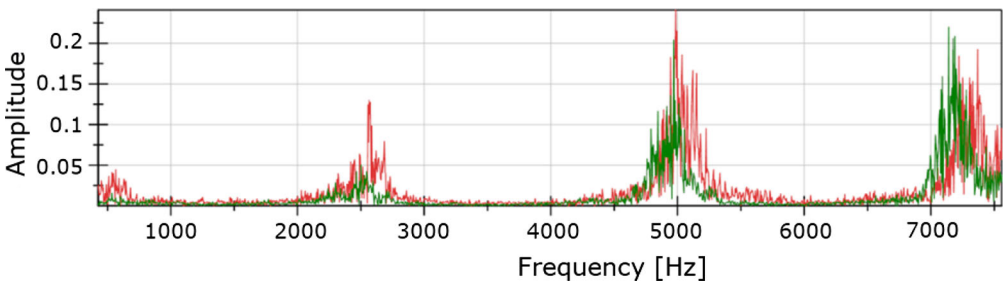

Fig. 16 Wave frequency spectrum: red—spectrum 1 (see Fig. 13), green—spectrum 2 (see Fig. 13), HFI

bustion mode most often between HFI and CRD. Unstable detonation occurred in a ~10 ms timescale when a detonation wave extinguished and transitioned through deflagration (or deflagrative combustion with HFI) back to CRD (see Figs. 13, 14, 15). In this work, unstable detonation correlated with relatively lower fresh reactant velocity inflow. High-frequency pressure records feature acoustic patterns or indistinct pressure peaks; however, this could have been influenced by the location of pressure sensors. FFT analysis indicates different ranges of dominant frequencies for different time intervals (see Fig. 16). The wave speed reached 50–70% of V_{C-J}. Geometry in this case was limited to Variant B (see Fig. 1). Combustor performance for this mode of combustion was similar to HFI. The most distinctive feature of this combustion mode was that it was vague and indefinite in an attempt to assign it to a specified category.

In this case, the basic criteria were often in conflict—on the one hand, the pressure records featured low wave speed, but, on the other hand, amplitudes reached ~10 bar. During combustion, frequency temporally varied causing so-called waning waxing instabilities (see Fig. 14).

4 Analysis of results and comparison of combustion modes

Several experiments allowed to observe all aforementioned combustion modes during similar flow conditions ($\dot{m} = 1.1-1.2$ kg/s) and the same inlet cross-sectional area. Each mode observed in Fig. 17 corresponded to different outlet slit width, i.e., different $A8$.

Figure 18 illustrates typical differences in measured parameters (total outlet pressure and thrust) for different combustion modes while Fig. 19 shows PG calculated using (2) and specific thrust calculated according to (1) for several selected experiments with different combustion modes. Combustion chamber parameters for various combustion modes are then summarized in Fig. 20.

The pressure in the chamber varied according to the outlet cross-sectional area; however, the combustion mode was a major factor affecting those differences. For example, for detonation and deflagration, for the same mass flow rate the outlet total pressure records obtained for cold flow (see Fig. 16) showed a pressure difference of around 7%; however, during hot flow after ignition the difference reached 23%. This suggested that more complete combustion occurred for detonation than for deflagration—the combustor was presumably too short to achieve complete deflagrative combustion. Lower chamber pressure gives a lower level of throttling which results in measured pressure gain that is far better than for detonative combustion. However, the highest specific thrust was measured for detonative combustion. Worth mentioning is that detonation stability had an unnoticeable influence on the combustor performance, especially on specific thrust. An interesting fact is that achieving better detonation stability required high inflow velocity (achieved by greater outlet cross-sectional area with the same chamber height across all experiments, see Fig. 5) which amplified pressure losses (greater pressure drop between the combustor plenum and the chamber), see Table 1.

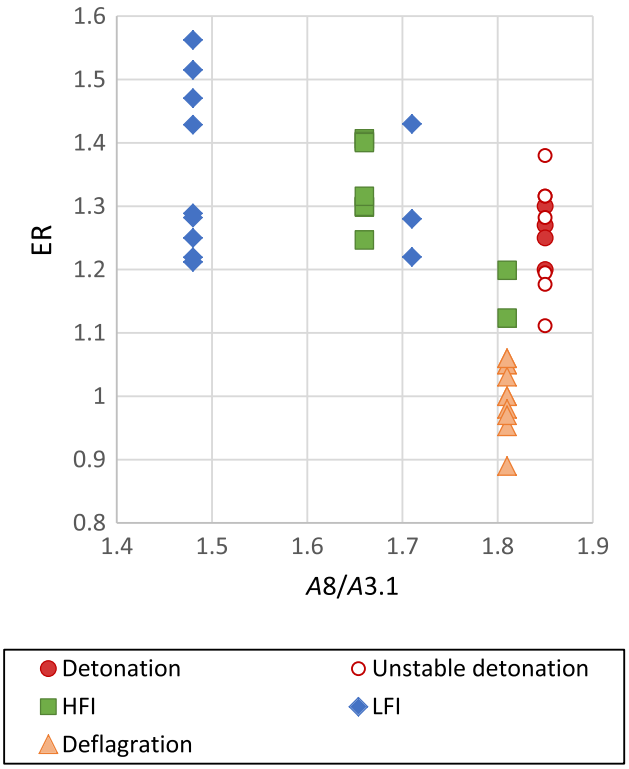

Fig. 17 Distribution of combustion modes for different values of geometric parameters $A8/A3.1$

5 Discussion

Stable detonation of a kerosene–air mixture requires satisfactory rate of kerosene droplet atomization, evaporation, and a high degree of mixing with the air. In this work, combustion of only rich mixtures was achieved, which indicates that part of the fuel was not atomized and evaporated.

In the studies presented, the cross-sectional area $A3.1$ was the same, and the different modes appeared at different choking conditions (different $A8$).

Attention is drawn to the large pressure loss in the detonation mode. For an "open" chamber—where $A8$ was large, conditions for stable detonation combustion were created. However, this geometric arrangement significantly worsened the aerodynamics of the chamber inlet. The detonation wave is located just behind the chamber inlet (slot 3.1), which blocks this inlet.

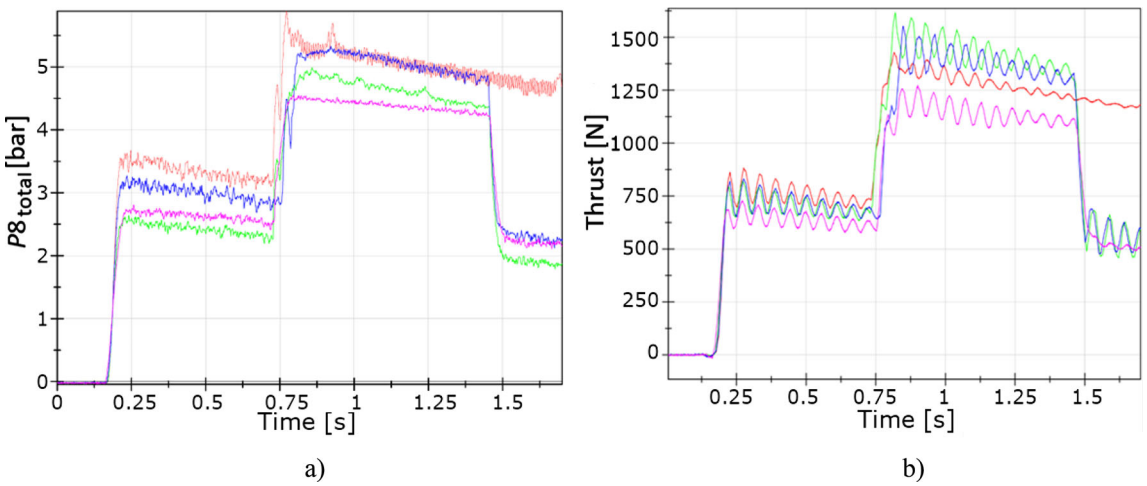

Fig. 18 Measured parameters of total outlet pressure (**a**) and thrust (**b**) for different combustion modes. Green—detonation; magenta—deflagration; red—LFI; blue—HFI

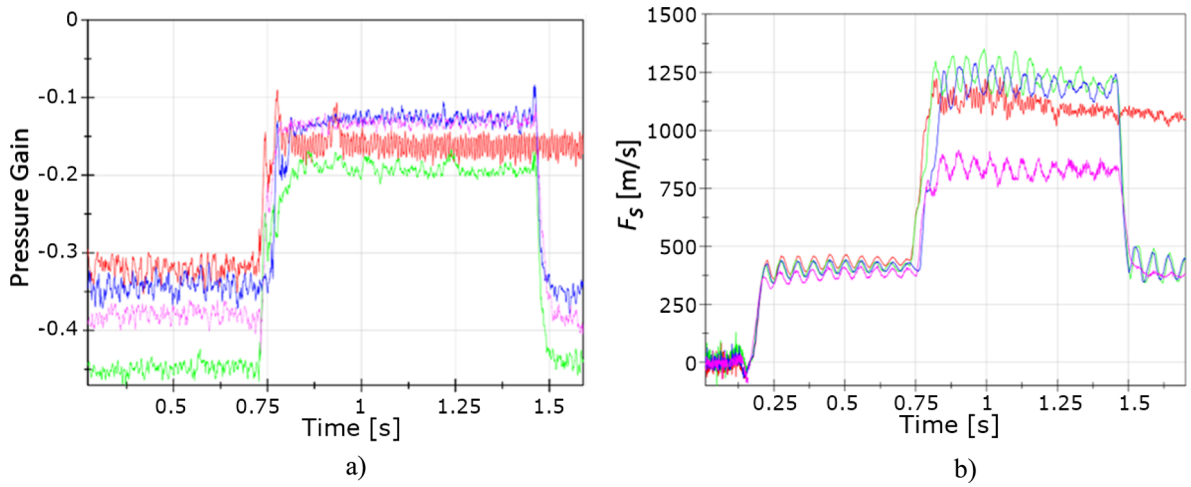

Fig. 19 Calculated (formulas in Sect. 2.2) parameters of pressure gain (**a**) and specific thrust (**b**) of combustion chamber for different combustion modes. Green—detonation; magenta—deflagration; red—LFI; blue—HFI

Table 1 Comparison of different combustion modes and the range of their parameters

Combustion mode	Chamber geometry	Mass flow rate (kg/s)	Pressure gain (%)	Specific thrust (m/s)
Stable detonation	Variant B	1.15 ÷ 1.26	− 23 ÷ − 19	1270 ÷ 1300
Unstable detonation	Variant B	1.13 ÷ 1.29	− 22 ÷ − 19	1180 ÷ 1300
HFI	Variant A and B	1.09 ÷ 1.19	− 16 ÷ − 13	1190 ÷ 1290
LFI	Variant A and B	1.10 ÷ 1.22	− 23 ÷ − 13	920 ÷ 1120
Deflagration	Variant A	1.09 ÷ 1.55	− 19 ÷ − 13	700 ÷ 940

The HFI mode performed surprisingly well. Good parameters of the combustion chamber parameters were observed—thrust and specific thrust close to detonation mode. Moreover, the flow parameters of the chamber were satisfactory. At this stage, it is difficult to determine the combustion mechanism of the HFI mode. There are local shock waves and acoustic waves appearing, interfering, and reflecting off each other and the chamber walls. Because the axial flow is too slow, it is not possible to obtain a sufficient layer of fresh mixture for the combustion to switch to the CRD mode. The pressure peaks are low (a few bars) and relatively wide (contrary to sharp peaks in detonation), and there is no blocking effect on the flow in the chamber.

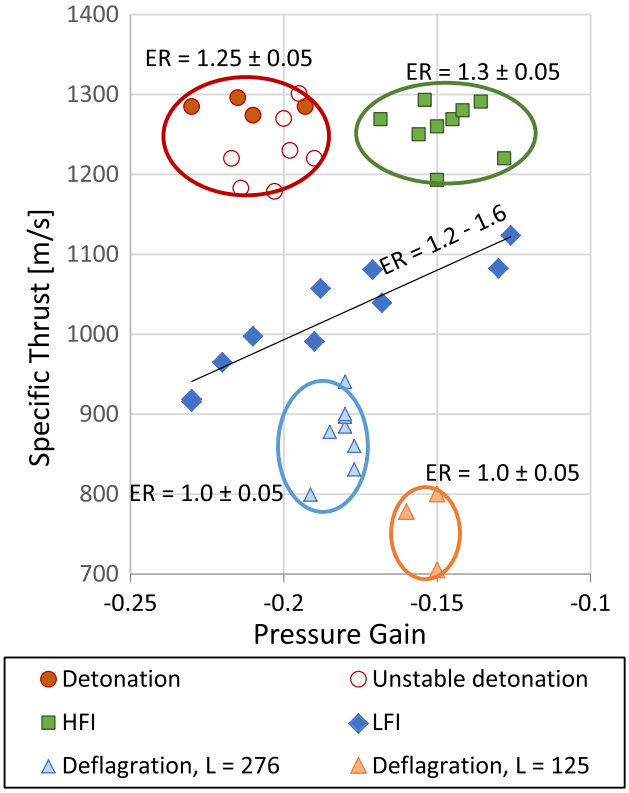

Fig. 20 Combustion chamber parameters for various combustion modes where a negative PG means total pressure losses

It is noteworthy that the combustion chamber geometry used for this work was aerodynamically not optimized, which contributed significantly to these losses, connected especially to the chamber inlet. Decrease in the aerodynamic losses is the key to obtaining much better propulsive performance. The fuel injection system refinement might also enhance the performance of the engine.

The length of the chamber ($L = 125$ mm) was insufficient for deflagration but was quite sufficient for other combustion modes, especially RD and HFI, which confirms that the use of detonative combustion processes allows for shortening the combustion chamber significantly.

In the determination of the specific thrust, the base drag was not measured and included in the total thrust. Otherwise, specific thrust would be increased by around 12% [5].

It was difficult to determine the conditions for which a stable detonation process would be achieved every time. Both stable detonation wave and unstable detonation wave occurred randomly under similar conditions.

6 Conclusions

In this work, experiments were conducted for the generic annular chamber with a diameter of $D = 141$ mm and the height of the chamber $h = 31$ mm. Several modes of combustion were recorded: from deflagration (observed only for geometry variant A) to low- and high-frequency combustion instabilities (for both geometry variants). Only for geometry variant B both stable detonation and unstable ("waning waxing") detonation were recorded. Very interesting is that the regions covered by different combustion modes obtained during the described tests are clearly separated from each other (see Fig. 20). During experiments, negligible influence of detonation stability on specific thrust was observed. Combustion with high-frequency instabilities featured a specific thrust comparable to detonation with lower pressure losses (but with higher ER, so higher fuel consumption). While detonation reached a PG of -19%, the combustion with high-frequency instabilities resulted in a PG up to -13%. Detonation combustion was located just behind the combustion chamber inlet gap blocking the flow; that resulted in flow losses and a reduced PG. Positive PG was not observed.

Acknowledgements The authors would like to express their appreciation to Elżbieta Zocłońska and Krzysztof Benkiewicz for fruitful discussions and relevant comments to this manuscript. This work was supported and funded by the Łukasiewicz Research Network—Institute of Aviation under statutory project no. 22157.

References

1. Teasley, T., Fedotowsky, T., Gradl, P., Austin, B., Heister, S.: Current state of NASA continuously rotating detonation cycle engine development. AIAA SciTech 2023 Forum, National Harbor, MD & Online, AIAA Paper 2023-1873 (2023). https://doi.org/10.2514/6.2023-1873
2. Wolański, P.: Detonative propulsion. Proc. Combust. Inst. **34**(1), 125–158 (2013). https://doi.org/10.1016/j.proci.2012.10.005
3. Kaemming, T.A., Paxson, D.E.: Determining the pressure gain of pressure gain combustion. 2018 Joint Propulsion Conference, Cincinnati, OH, AIAA Paper 2018-4567 (2018). https://doi.org/10.2514/6.2018-4567
4. Bach, E., Paschereit, C.O., Stathopoulos, P., Bohon, M.D.: An empirical model for stagnation pressure gain in rotating detonation combustors. Proc. Combust. Inst. **38**(3), 3807–3814 (2022). https://doi.org/10.1016/j.proci.2020.07.071
5. Bach, E., Stathopoulos, P., Paschereit, C.O., Bohon, M.D.: Performance analysis of a rotating detonation combustor based on

stagnation pressure measurements. Combust. Flame **217**, 21–36 (2020). https://doi.org/10.1016/j.combustflame.2020.03.017
6. Brophy, C.M., Codoni, J.R., Teneyck, J.A., Ewing, S.: Experimental performance characterization of an RDE using equivalent available pressure. AIAA Propulsion and Energy 2019 Forum, Indianapolis, IN, AIAA Paper 2019-4212 (2019). https://doi.org/10.2514/6.2019-4212
7. Sousa, J., Paniagua, G., Morata, E.C.: Thermodynamic analysis of a gas turbine engine with a rotating detonation combustor. Appl. Energy **195**(1), 247–256 (2017). https://doi.org/10.1016/j.apenergy.2017.03.045
8. Wolański, P., Kalina, P., Balicki, W., Rowiński, A., Perkowski, W., Kawalec, M., Łukasik, B.: Development of gas turbine with detonation chamber. In: Li, J.-M., Teo, C.J.T., Khoo, B.C., Wang, J.-P., Wang, C. (eds.) Detonation Control for Propulsion, pp. 23–37. Springer, Cham (2017). https://doi.org/10.1007/978-3-319-68906-7_2
9. Le Naour, B., Davidenko, D., Gaillard, T., Vidal, P.: Rotating detonation combustors for propulsion: some fundamental, numerical and experimental aspects. Front. Aerosp. Eng. Sect. Energ. Propuls. (2023). https://doi.org/10.3389/fpace.2023.1152429
10. Naples, A., Fotia, M., Theuerkauf S., Hoke, J.L., Schauer, F.R.: Design and testing of a rotating detonation engine for open-loop gas turbine integration. 25th International Colloquium on the Dynamics of Explosions and Reactive Systems, Leeds, UK, Paper 19 (2015)
11. Baratta, A.R., Stout, J.B.: Demonstrated low pressure loss inlet and low equivalence ratio operation of a rotating detonation engine (RDE) for power generation. AIAA SciTech 2020 Forum, Orlando, FL, AIAA Paper 2020-1173 (2020). https://doi.org/10.2514/6.2020-1173
12. Xue, S., Ying, Z., Ma, H., Zhou, C.: Experimental investigation on two-phase rotating detonation fueled by kerosene in a hollow directed combustor. Front. Aerosp. Eng. Sect. Adv. Clean Fuel Technol. **10**, 25 (2022). https://doi.org/10.3389/fenrg.2022.951177
13. Zheng, Q., Meng, H.L., Weng, Ch., Wu, Y., Feng, W., Wu, M.: Experimental research on the instability propagation characteristics of liquid kerosene rotating detonation wave. Def. Technol. **16**(6), 1106–1115 (2020). https://doi.org/10.1016/j.dt.2020.06.028
14. Zhou, J., Song, F., Wu, Y., Xu, S., Yang, X., Cheng, P., Li, Y.: Investigation of pressure gain characteristics for kerosene-hot air RDE. Combust. Flame **247**, 112503 (2023). https://doi.org/10.1016/j.combustflame.2022.112503
15. Kindracki, J.: Experimental research on rotating detonation in liquid fuel-gaseous air mixtures. Aerosp. Sci. Technol. **43**, 445–453 (2015). https://doi.org/10.1016/j.ast.2015.04.006
16. Anand, V., Gutmark, E.: Rotating detonation combustors and their similarities to rocket instabilities. Prog. Energy Combust. Sci. **73**, 182–234 (2019). https://doi.org/10.1016/j.pecs.2019.04.001
17. Anand, V., George, A.S., Driscoll, R., Gutmark, E.: Longitudinal pulsed detonation instability in a rotating detonation combustor. Exp. Therm. Fluid Sci. **77**, 212–225 (2016). https://doi.org/10.1016/j.expthermflusci.2016.04.025
18. Heiser, W.H., Pratt, D.T.: Hypersonic Airbreathing Propulsion, AIAA Education Series. Washington, DC (1994). https://doi.org/10.2514/4.470356
19. Rupperecht, S., Faeth, G.: Investigation of air solubility in jet A fuel at high pressures. NASA Contract. Rep. **3422**, 33 (1981)
20. Perkowski, W., Irzycki, A., Snopkiewicz, K., Grudzień, Ł, Kawalec, M.: Study on kerosene atomization process under a high-speed air stream. J. KONES Powertrain Transp. **18**(4), 341–347 (2011)
21. Xie, Q., Wang, B., Wen, H., He, W.: Thermoacoustic instabilities in an annular rotating detonation combustor under off-design condition. J. Propuls. Power **35**(1), 28 (2018). https://doi.org/10.2514/1.B37044
22. Kindracki, J.: Study of detonation initiation in kerosene-oxidizer mixtures in short tubes. Shock Waves **24**, 603–618 (2014). https://doi.org/10.1007/s00193-014-0519-2
23. Wang, F., Weng, Ch., Wu, Y., Bai, Q., Zheng, Q., Xu, H.: Effects of total pressures and equivalence ratios on kerosene/air rotating detonation engines using a paralleling CE/SE method. Defence Technol. **17**(6), 1805–1816 (2021). https://doi.org/10.1016/j.dt.2020.09.015